Clinical and Translational Radiation Oncology 42 (2023) 100662

Contents lists available at ScienceDirect

Clinical and Translational Radiation Oncology

journal homepage: www.sciencedirect.com/journal/clinical-and-translational-radiation-oncology

A time-resolved clonogenic assay for improved cell survival and RBE measurements

Robin A Koch [a,b,c,d,*], Marc Boucsein [a,b,c,d], Stephan Brons [b,e], Markus Alber [a,b,c], Emanuel Bahn [a,b,c,d]

[a] Department of Radiation Oncology, Heidelberg University Hospital, Im Neuenheimer Feld 672, 69120 Heidelberg, Germany
[b] Heidelberg Institute of Radiation Oncology (HIRO), Im Neuenheimer Feld 280, 69120 Heidelberg, Germany
[c] National Center for Tumor Diseases (NCT), Im Neuenheimer Feld 460, 69120 Heidelberg, Germany
[d] Clinical Cooperation Unit Radiation Oncology, German Cancer Research Center (DKFZ), Im Neuenheimer Feld 280, 69120 Heidelberg, Germany
[e] Heidelberg Ion-Beam Therapy Center (HIT), Department of Radiation Oncology, Heidelberg University Hospital, Im Neuenheimer Feld 450, 69120 Heidelberg, Germany

ARTICLE INFO

Keywords:
Radiobiology
Dose-response relationship, radiation
Relative biological effectiveness
Heavy ion radiotherapy
Time-lapse imaging
Supervised machine learning

ABSTRACT

Purpose: The in vitro clonogenic assay (IVCA) is the mainstay of quantitative radiobiology. Here, we investigate the benefit of a time-resolved IVCA version (trIVCA) to improve the quantification of clonogenic survival and relative biological effectiveness (RBE) by analyzing cell colony growth behavior.
Materials & Methods: In the IVCA, clonogenicity classification of cell colonies is performed based on a fixed colony size threshold after incubation. In contrast, using trIVCA, we acquire time-lapse microscopy images during incubation and track the growth of each colony using neural-net-based image segmentation. Attributes of the resulting growth curves are then used as predictors for a decision tree classifier to determine clonogenicity of each colony. The method was applied to three cell lines, each irradiated with 250 kV X-rays in the range 0–8 Gy and carbon ions of high LET (100 keV/µm, dose-averaged) in the range 0–2 Gy. We compared the cell survival curves determined by trIVCA to those from the classical IVCA across different size thresholds and incubation times. Further, we investigated the impact of the assaying method on RBE determination.
Results: Size distributions of abortive and clonogenic colonies overlap consistently, rendering perfect separation via size threshold unfeasible at any readout time. This effect is dose-dependent, systematically inflating the steepness and curvature of cell survival curves. Consequently, resulting cell survival estimates show variability between 3% and 105%. This uncertainty propagates into RBE calculation with variability between 8% and 25% at 2 Gy.
Determining clonogenicity based on growth curves has an accuracy of 95% on average.
Conclusion: The IVCA suffers from substantial uncertainty caused by the overlap of size distributions of delayed abortive and clonogenic colonies. This impairs precise quantification of cell survival and RBE. By considering colony growth over time, our method improves assaying clonogenicity.

Introduction

The in vitro clonogenic assay (IVCA), developed over 60 years ago [1], is a fundamental tool to quantify dose-dependent changes in cells' proliferative capacities after irradiation and hence has been an indispensable assay in radiobiology for the last decades. For reasons of feasibility and interpretability, this assay reduces the complex growth behavior of cell colonies to a scalar readout, i.e. a dose-dependent survival rate. This allows quantification and comparison of radiation-induced cell death in a multitude of different conditions with relative ease.

However, results acquired with this method vary substantially between different studies and experiments [2,3]. Multiple sources for this variability were investigated, such as human error [4,5] and differences in the experimental protocol. Notable effects were found for seeding densities [6], pre-treatment culture conditions [7], and seeding times [8].

Our motivation to add the time dimension to this assay is threefold:

* Corresponding author at: Department of Radiation Oncology, Heidelberg University Hospital, Im Neuenheimer Feld 672, 69120 Heidelberg, Germany.
E-mail addresses: robin.koch@dkfz-heidelberg.de (R.A. Koch), marc.boucsein@dkfz-heidelberg.de (M. Boucsein), stephan.brons@med.uni-heidelberg.de (S. Brons), markus.alber@med.uni-heidelberg.de (M. Alber), e.bahn@dkfz-heidelberg.de (E. Bahn).

https://doi.org/10.1016/j.ctro.2023.100662
Received 3 March 2023; Received in revised form 20 June 2023; Accepted 20 July 2023
Available online 22 July 2023

a) By condensing the experiment into a scalar survival rate, information about colony growth processes is lost. By studying the growth behavior of colonies, we hope to identify systematic biases inherent in the IVCA method and separate them from true biological effects.

b) In certain applications, such as RBE determination, highly accurate estimates for clonogenic survival are the foundation for reliable clinical models. To enable rational treatment decisions in the clinic, uncertainty in dose effectiveness is required to be smaller than 5%. Naturally, parameters informing these models, such as RBE, need to be determined at least as precisely. By considering growth dynamics, we aim for a more robust classification of clonogenicity, and thereby a more precise determination of survival and survival-based quantities such as RBE and dose-modifying factors.

c) Automated imaging, high-throughput image processing, and computer-assisted detection and classification of colonies are necessary prerequisites for the presented method, but they enhance throughput substantially, allowing for a strong data foundation.

In recent work [9] we have shown the technical feasibility of time-resolved growth analysis after irradiation. Here, we focus on the tangible benefits of using this method compared to the classical IVCA.

We present a method that extends the IVCA to a time-resolved IVCA (trIVCA) with the capacity to examine the full growth history of thousands of colonies throughout the complete incubation time. We quantify differences between the approaches and show the benefits of the time-resolved analysis.

Materials and methods

Cell culture and treatment

The trIVCA analysis was performed on three cell lines: H460 (human, large cell lung carcinoma), UTSCC5 (human, squamous cell carcinoma of the tongue), and RENCA (murine, renal adenocarcinoma) to cover different tumor types, species and doubling rates.

All cell lines were cultured in RPMI 1640 + 10% FCS + 1% PenStrep at 37 °C, 5% CO_2. Treatment was performed following the "plating after treatment" protocol as described by Franken et al. [10]. To prepare the treatment, identical numbers of cells ($\sim 10^3$) were seeded into T12.5 culture flasks, using as many flasks as there were conditions to be tested, and incubated at 37 °C and 5% CO_2. The relatively sparse initial seeding ensures a long growth period before irradiation, minimizing potential cell cycle synchronization effects at irradiation time.

Irradiation

Flasks were irradiated when the cells reached confluence levels of ~70%. For each cell line, we performed two comparative trIVCA experiments in parallel, one after photon irradiation (5 doses in the range from 0 Gy to 8 Gy) and one after carbon ion irradiation (5 doses in the range from 0 Gy to 2 Gy). These doses were chosen to cover a range in which we would still expect to find sufficient numbers of surviving colonies, despite the relatively low seeding density. Comparisons between photon and carbon doses were based on an RBE of 4.0, as reported for the H460 cell line by Bronk et al. [11].

Photon irradiation was performed in a Faxitron Multirad 225 (Faxitron Bioptics, Tucson, Arizona, USA; settings: 200 kV X-rays, 0.5 mm Cu filter, dose rate 1 Gy/min). Carbon ion irradiation was performed at the Heidelberg Ion Beam Therapy Center (HIT) experiment beamline (dose-averaged LET 100 keV/µm, averaged dose rate 2.0 Gy/min). Photon and carbon irradiation were performed on the same day with an offset of 1.5 h due to handling times. Directly after irradiation, cells were harvested, counted, and seeded in T25 cell culture flasks at identical densities between 300 and 800 cells per flask, depending on the expected growth rate of the cell line. The relatively low seeding number was chosen to avoid coalescence of colonies during growth, as this can impede true single-colony analysis for late time points. For each dose, three replicate flasks were seeded. After 4 h, cells were fully attached and initial imaging was performed.

Imaging

For every dataset, time-course microscopy images were acquired every 24 h for 11 days, using a Zeiss Axio CellObserver microscopy system equipped with temperature and CO_2 incubation. Settings were controlled using the ZEN 2 (blue edition) software. Contrast images were acquired using differential interference contrast imaging at 2.5X magnification by tile-imaging over the complete flask. The z-levels for imaging were defined based on a "global focus surface". This focus surface was calculated by ZEN 2 for each flask and each imaging round based on four support points, which we defined visually. Flasks were kept at 37 °C and 5% CO_2 throughout the imaging period *(*Fig. 1*a)*.

Image analysis

The micrograph tiles were processed in ImageJ by stitching all tiles into a single image using the Microscopy Image Stitching Tool (MIST) stitching algorithm [12]. Subsequent image registration was performed to align all images of a given replicate flask to ensure robust location-based tracking. We used the SimpleElastix (v0.10.0) toolbox implemented in the SimpleITK (v2.2.0) module for python [13,14]. To minimize the influence of imaging artifacts on the registration, it was restricted to the rim area of the flask images. Configuration files defining the registration settings and Python scripts executing the registration will be made available upon request to the author.

After registration, the images were segmented using a UNet-based deep learning model that was built and trained using the nnUNet toolbox [15]. The model was trained on 50 fully labeled, representative image sections. These sections were taken from random locations of random images containing different cell lines (H460, UTSCC5 and RENCA) after receiving different doses (0–8 GyE) of both modalities (photons and carbon ions) after incubation for different durations (0–240 h). This variability in the training data was introduced to obtain a well-generalizing model. The labels were created manually in the interactive visualization framework napari [16]. Training of the model and segmentation of the images were performed using GPU-accelerated computing on the DKFZ cluster. Following the segmentation, separation of fused colonies was performed by applying distance transform and watershed transform on the binary segmentation masks *(*Fig. 1*b)*.

Colony tracking

Based on the binary segmentation masks, we tracked all objects using a location-based approach. Every object refers to a contiguous region within an image that is marked as colony by the segmentation algorithm. We refer to these objects as colony objects, even though they might contain only a single cell: For each colony object C in an image at time t, the distance to all colony objects in the next image at time t + 1 is calculated based on the objects' centroids. If the distance between this object C and the closest object at time t + 1 is below a user-chosen threshold, this closest object is attached to the track containing object C. Tracking quality was validated by visually confirming correctness on several hundreds of tracks, randomly chosen from different cell lines, doses, and replicates *(*Fig. 1*c)*.

Growth behavior classification

Growth behavior classifiers were created individually for each cell line. To classify the clonogenicity of a growing colony, we used a decision tree classifier with predictors MaxSize and MaxTime, where MaxSize is the largest size a colony reaches throughout its growth and MaxTime is the time at which this size is reached. We trained the classifier using a subset of 250 tracks for each cell line. To ensure balanced

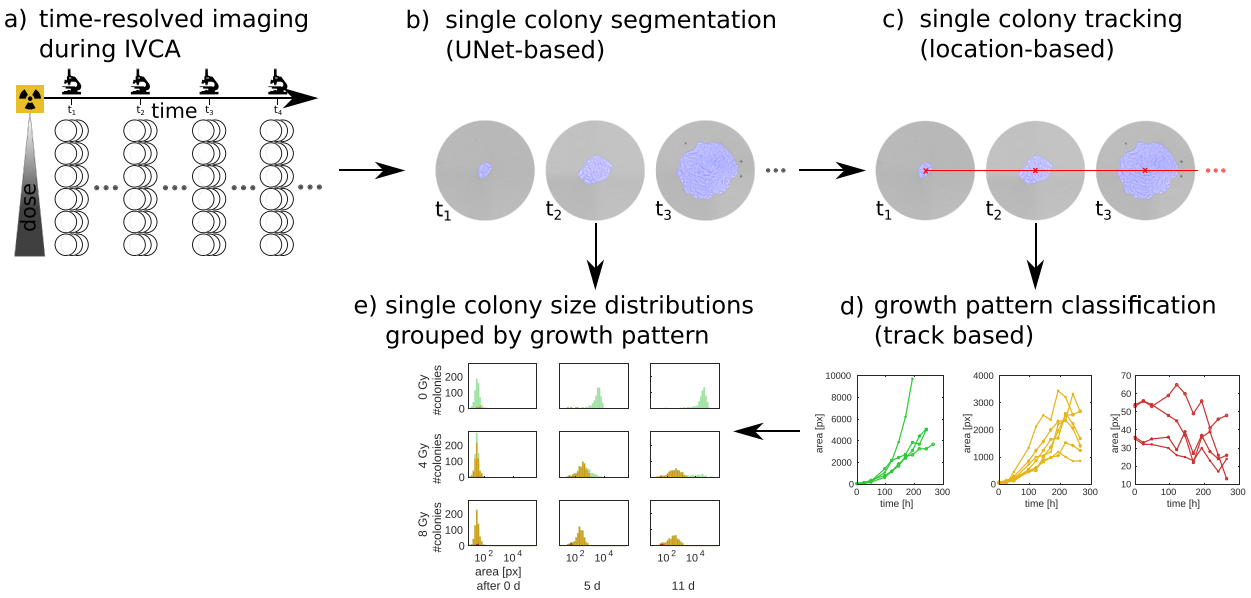

Fig 1. Data analysis overview. a) Time-course microscopy images of complete cell culture containers are acquired during incubation. b) For every image, all colonies are detected and quantified using a UNet-based segmentation and c) single colony growth is tracked through time based on location. d) Every colony is classified regarding their growth pattern, yielding e) distributions of colony sizes mapped to their growth patterns across time and doses. Green, yellow and red represent clonogenic, delayed abortive and initially abortive colonies, respectively. (For interpretation of the references to colour in this figure legend, the reader is referred to the web version of this article.)

training data, this subset was defined to contain identical numbers of tracks from each dose, with the tracks chosen randomly for each dose. Every track in this training set was labeled manually as one of the three growth behavior classes [*abortive, delayed abortive, clonogenic*]. This was achieved by displaying a movie of the full growth dynamics of the colony to the user, who then labeled the colony track accordingly. After all training tracks were labeled, the classifier was trained on those tracks. To realistically assess performance and potential sampling biases, 5-fold cross-validation was used.

Prediction accuracies of 95.6 +- 0.3% for H460, 96.1 +- 0.7% for RENCA, and 93.7 +- 0.4% for UTSCC5 were achieved. These values represent the mean +- standard errors of 1000 cross-validation accuracies. Each of these accuracies was obtained by performing 5-fold cross-validation based on random, independent splits of the same training data.

The resulting classifiers were used to classify the growth behavior of every single colony in the respective datasets *(*Fig. 1*d)*. By mapping growth behavior of individual colonies back to their sizes at different times (Fig. 1*e*), the distribution of colony sizes grouped by growth behavior yields insights into how well these subpopulations separate in terms of size and how large the potential misclassification is; i.e. how many clonogenic, but slowly growing, hence small colonies (false negatives) are present and how many delayed abortive, but large colonies (false positives) are present at different doses?

Survival calculation

The threshold-based calculation of dose-dependent survival was performed as described in Franken2006[10], except the number of initially seeded cells was not estimated based on the dilution protocol, but determined for every replicate by automatically counting the number of single cells present in the first image. Colonies counted as clonogenic are colonies displaying a size greater than a user-defined size threshold at readout time. To estimate cell numbers per colony, a mapping between colony size and cell count was created by robust linear regression of visually determined cell counts against their corresponding sizes for 300 colonies per cell line. This allows the definition of colony size thresholds which correspond to standard readout cell numbers.

Dose-dependent survival fractions based on growth behavior classification ($F_g(D)$) were calculated as

$$F_g(D) = \frac{N_{c,D}}{N_{t,D}},$$

where $N_{c,D}$ is the number of single-colony growth curves classified as clonogenic at dose D and $N_{t,D}$ is the total number of single-colony growth curves captured for that dose. As in the standard IVCA, relative survival $S_g(D)$ was calculated by normalizing the dose-dependent survival fraction $F_g(D)$ to the survival fraction at 0 Gy $F_g(0)$:

$$S_g(D) = F_g(D)/F_g(0)$$

Survival curves were defined based on the linear-quadratic model, with model parameters α and β determined by a nonlinear least-squares fit to all replicate (log-)survival values.

RBE calculation

Given the LQ parameters of two survival curves, the reference-dose-dependent RBE was calculated as

$$RBE(D_R) = \frac{-2\beta_C D_R}{\alpha_C - \sqrt{\alpha_C^2 - 4\beta_C{}^*\left(-\alpha_R D_R - \beta_R D_R^2\right)}}$$

where DR is the photon reference dose, α_R and β_R are the LQ parameters of the reference curve and α_C and β_C are the LQ parameters of the comparison curve (here carbon ions with LET = 100 keV/μm).

Results

We applied the analysis to three different cell lines, each irradiated with photons and carbon ions. The acquired colony size distributions (Fig. 2, other cell lines Fig. S1) contain a multitude of information:

A) The distribution of colony sizes propagates towards larger sizes with time, displaying the population colony growth. This shift occurs at different rates for different cell lines, illustrating different mean growth rates between cell lines.

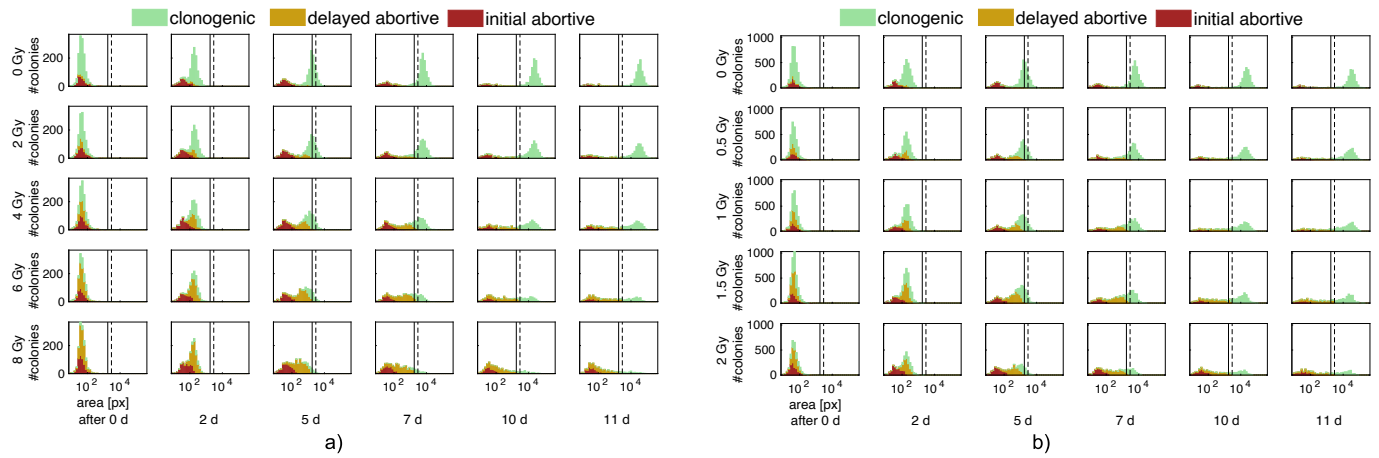

Fig 2. Colony size distributions at multiple time points at each dose. Note the logarithmic x-axes. Results for cell line RENCA. For other cell lines, see Supplement Fig. S1. a) After photon irradiation. b) after carbon ion irradiation. Vertical lines represent size thresholds for 30 (solid) and 50 (dashed) cells, respectively. Colors represent growth behavior classification: red – initially abortive; yellow – delayed abortive; green – clonogenic. (For interpretation of the references to colour in this figure legend, the reader is referred to the web version of this article.)

B) Without irradiation (0 Gy), clonogenic and non-clonogenic colonies can be separated based solely on colony size after some time: they form a bimodal distribution with a close-to-zero minimum between the peaks. This is true for all tested cell lines.
C) With increasing irradiation dose, this separation becomes less clear. All sizes are present to some extent. The magnitude of this effect is comparable between photon and carbon datasets for each cell line but varies between the cell lines.
D) The issue of uncertain size-based clonogenicity classification is resolved by instead performing a growth behavior classification based on single-colony growth dynamics.

As shown in Figs. 3 and S2, for standard readout times (7, 10, or 11 days) and standard threshold sizes (30, 40, or 50 cells), we found variations (i.e. relative standard errors) in apparent survival in the range of at least 3% (UTSCC5, photon, 1 Gy) to up to 105% (UTSCC5, photon, 6 Gy).

As depicted in Fig. 4, misestimations relative to growth behavior-based survival vary between + 13% (RENCA, carbon, 4 Gy) and −88% (H460, photon, 8 Gy). Notably, we cannot find a combination of readout time and threshold size for any cell line and modality that approximates the survival rates found by growth behavior classification within a 5% range. In addition, we observe some general trends:

Generally, the time-fixed, threshold-based approach underestimates survival compared to growth behavior-based survival, with 186/270 (69%) of standard survival values below the growth behavior-based survival across all cell lines, modalities, and doses.

Underestimation of survival is generally stronger at earlier time points compared to later time points (average underestimation 7d: −28%; 10d: −19%; 11d: −14%).

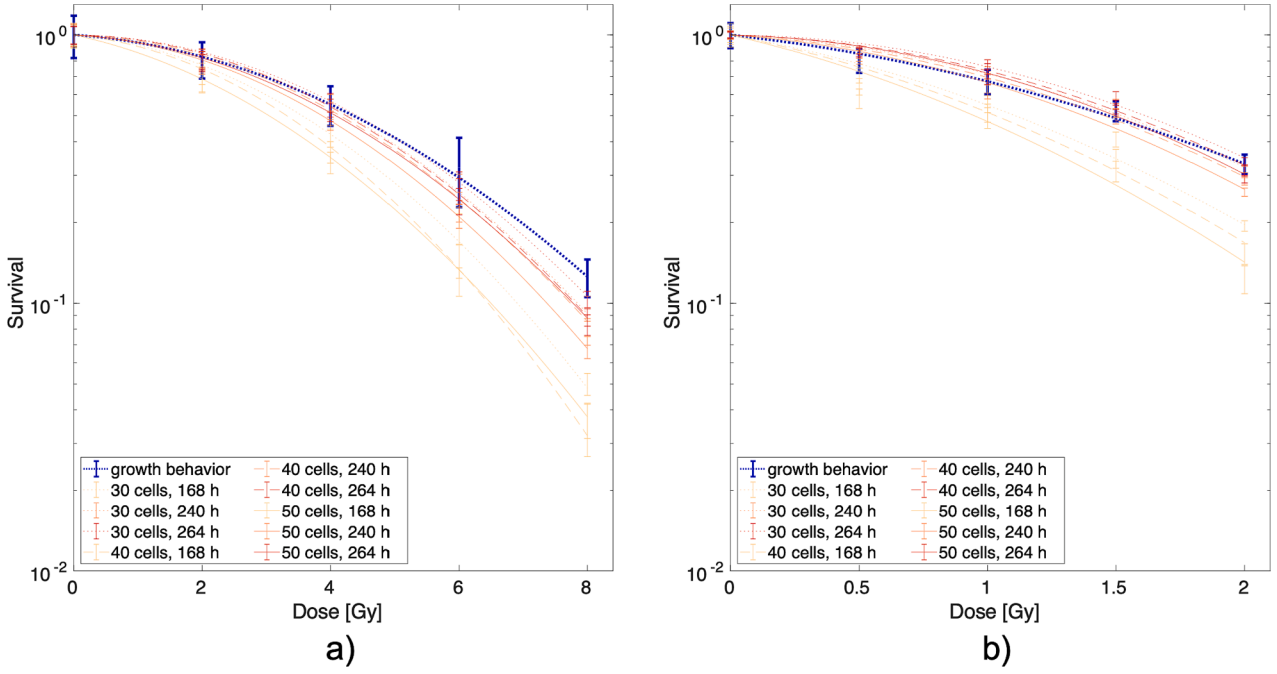

Fig 3. Survival curve fits based on different readout thresholds or based on growth behavior classification. Results for cell line RENCA. For other cell lines, see Supplement Fig. S2. a) survival curves and fits after photon irradiation. b) survival curves and fits after carbon irradiation. Error bars represent mean +- SD over the replicates. Curved lines depict LQ fits to the respective survival fractions.

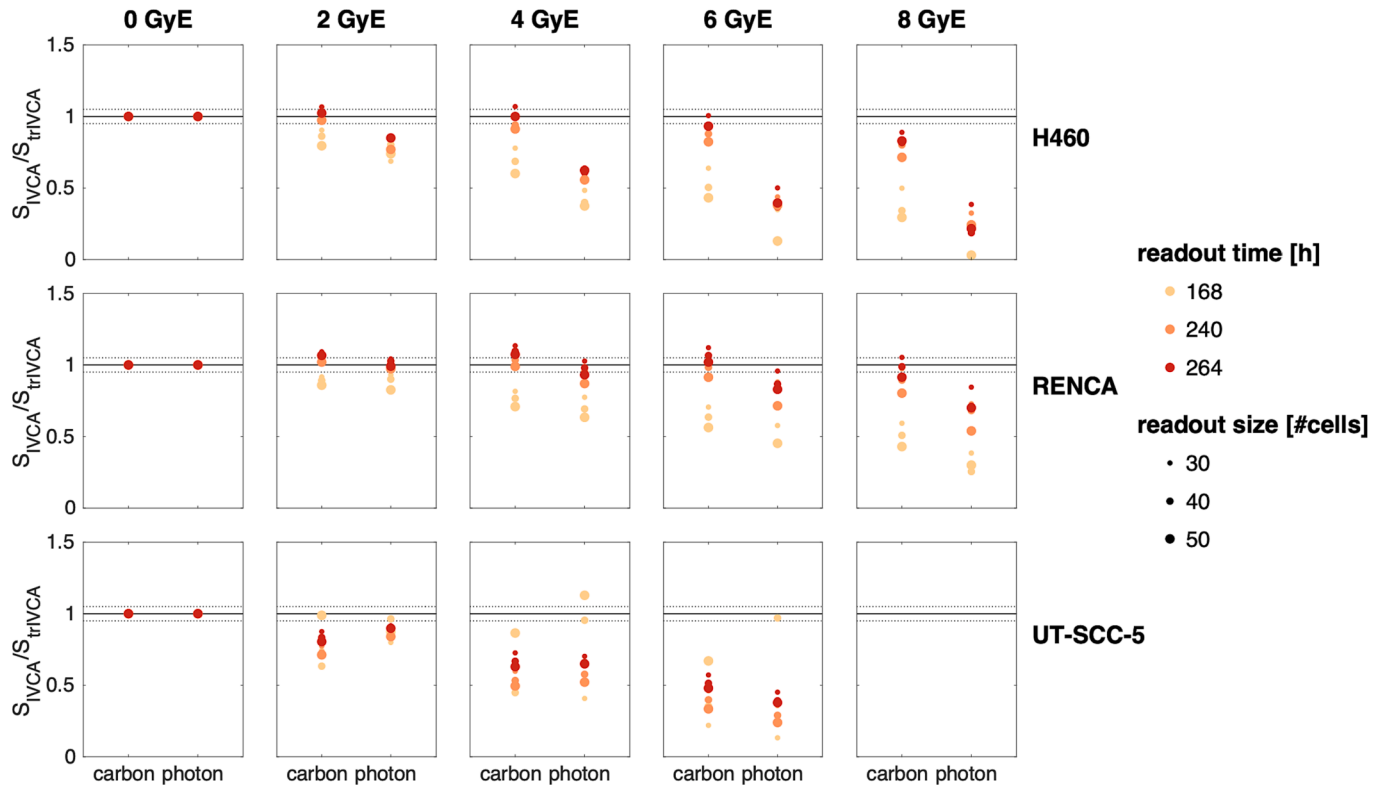

Fig 4. Threshold-based survival values relative to growth behavior-based survival values. For each cell line (rows) and each dose equivalent (columns, equivalence based on RBE = 4), for both photon and carbon samples, the values are determined by dividing the standard IVCA survival values for different readout times and colony size thresholds by the survival values from the trIVCA analysis. Different colors indicate different readout times, different marker sizes indicate different readout sizes. The solid line represents identity, with dashed lines above and below representing the +- 5% interval.

Underestimation of survival increases for higher doses (average underestimation 2GyE: −10%; 4GyE: −24%; 6GyE: −37%; 8GyE: −44%).

Underestimation of survival is generally stronger for photon-irradiated samples compared to carbon-irradiated samples (average underestimation photon: −26%, carbon: −15%).

Naturally, trends a) to c) result in generally higher values of the LQ-parameter beta for the standard approach compared to the growth behavior-based approach (Fig S3), representing steeper, more bent curves.

In combination with trend d), these effects also bleed into RBE quantification. In the following, whenever the term RBE is used, it implies RBE(carbon ions, LET = 100 keV/µm).

Using pairs of survival curves from both modalities, acquired using a given set of readout parameters, we calculated RBE as a function of (photon) reference dose for different choices of readout parameters (see Eq 1). Analogously, we calculated RBE based on the growth-based survival curves. As shown in Figs. 5 and 6, dose-dependent RBE values vary strongly among the threshold-derived results. For each cell line, we find over- as well as underestimated RBE curves relative to the growth behavior-based results. The RBE values determined at the clinically

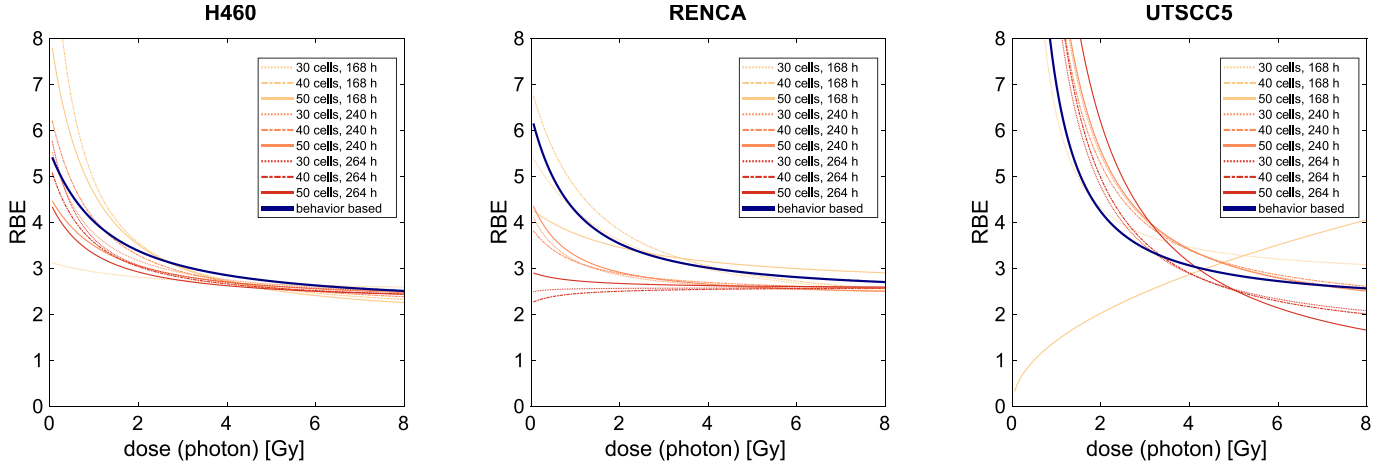

Fig 5. RBE vs reference dose for the three cell lines, calculated from linear-quadratic fits to the clonogenic survival curves. Survival was determined either based on growth classification (thick, dark blue line) or based on the classical IVCA with different readout thresholds (thin, red to yellow lines) for comparison. (For interpretation of the references to colour in this figure legend, the reader is referred to the web version of this article.)

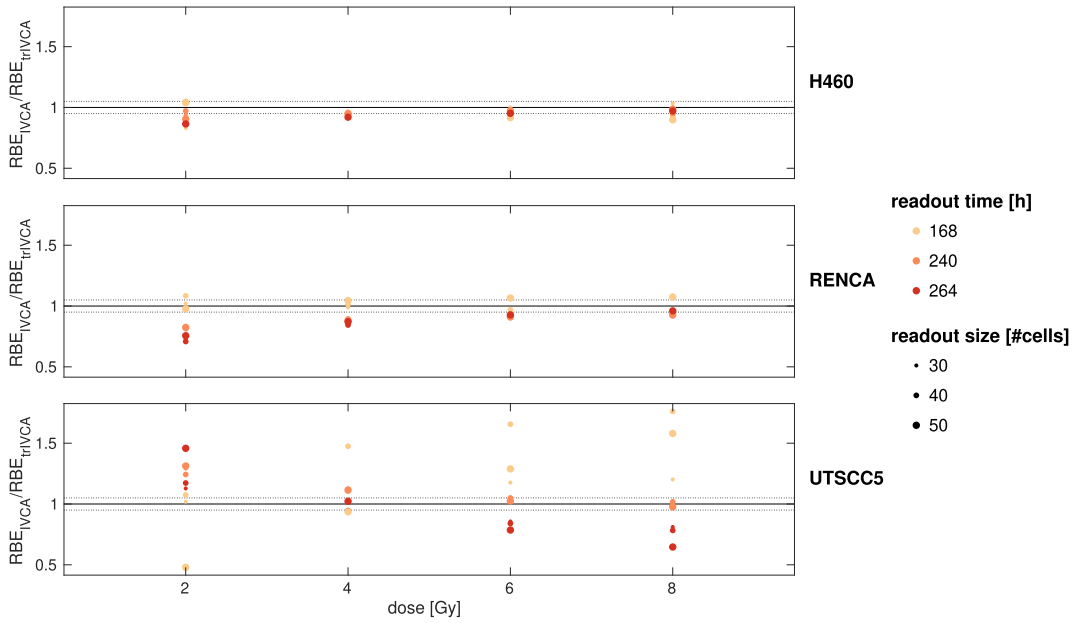

Fig 6. Threshold-based RBE values relative to growth behavior-based RBE values. For all cell lines (rows) and all (photon) reference doses, the values are determined by dividing the standard IVCA RBE values for different readout times and colony size thresholds by the RBE values from the trIVCA analysis. Different colors indicate different readout times, different marker sizes indicate different readout sizes. The solid line represents identity, with dashed lines above and below representing the +- 5% interval.

relevant 2 Gy level vary between 2.8 and 3.6 for H460 (growth behavior-based: 3.4), between 2.5 and 3.8 for RENCA (growth behavior-based: 3.5), and between 2.0 and 6.1 for UTSCC5 (growth behavior-based: 4.2). For UTSCC5, it is worth noting the threshold-based result for 50 cells after 168 h, which shows a trend opposing all other readouts, as RBE increases with increasing dose. For all other readouts, results show high (>5) RBEs at low doses (<2 Gy).

Discussion

As reasoned by Puck, Marcus, and others [1,10,17], colony size at readout times between 7 and 14 days is an informative predictor of clonogenicity. However, using our time-resolved assay, we found a substantial portion of misclassified colonies at these times. Some colonies grow over the threshold but then stop, others grow steadily, but too slowly to reach the threshold in time. This finding is in line with earlier research about slowly growing, clonogenic colonies [9,18–20].

Many potential sources of variability in the IVCA-based determination of cell survival curves are known, such as human readout variability, seeding densities, pre-treatment culture conditions, and seeding times [2–8]. Here we show that variations in readout time and size threshold choices are factors adding to this variability. Given the magnitude of variation observed, the standard IVCA approach seems to be a non-optimal choice, as we aim at precise clonogenic survival quantification to inform RBE or dose modification models.

Considering more relevant information by analyzing time-resolved growth is a natural improvement over restricting the analysis to fixed snapshots. It also enables us to examine dose- or condition-dependent effects on more detailed aspects of colony behavior: not just final colony sizes, but size distributions, growth behaviors, and growth rates.

Since the presented method utilizes automated machine-learning approaches to analyze the data, it enables us to process large amounts of data and yield quantitative results on a statistically solid foundation. This shows in the growth behavior classification accuracies of around 95% for all cell lines.

In addition to a more accurate clonogenicity classification, the abundance of data available in the time-resolved IVCA allows for a comprehensive quality inspection of performed experiments. This can help to gauge whether the measurements by the IVCA suffer from statistical or systematic errors and if cell lines, durations, seeding concentrations, and other experimental conditions are suitable for a classical IVCA analysis.

In the presented experiments, in addition to the readout-based variability, we determined a systematic misclassification trend in the standard approach: in all studied cell lines, size-based classification methodically underestimates clonogenic survival rates in the classical IVCA. With increasing dose, this underestimation increases as the population mean growth rates decrease, resulting in a higher number of slowly growing but clonogenic colonies [9]. This dose-dependent effect increases the curvature of the determined cell survival curves and brings about overestimated LQ beta compared to the growth behavior-based clonogenic survival quantification.

Unsurprisingly, the observed trends also affect the quantification of RBE, as the variability shown in Fig. 5 demonstrates. These findings might be one explanation why in vitro-based RBE measurements suffer from a large variability, which leads to large uncertainty in RBE models, particularly in the case of protons [2]. Using the growth behavior-based definitions of clonogenic survival, we can avoid the readout-dependent biases introduced by the misclassification of colonies, resulting in a more robust determination of clonogenic survival and subsequently RBE values.

In addition to the trends mentioned above, the UTSCC5 results in Fig. 5 yield additional insight: The “outlier” curve (50 cells, 168 h), representing a (too) early readout with a large size threshold, shows how inappropriate readout choices can lead to nonsensical results, as it is known that RBE decreases with increasing dose [21]. In addition, we observe that UTSCC5 behaves distinctly different to the two modalities at low doses: A clear shoulder in the survival curve after photon irradiation (Fig S2c) and a relatively flat survival curve after carbon ion irradiation (Fig S2d) lead to large RBE values in this dose range. Biological reasons for this are unclear.

In terms of clinical relevance, it is known, that in vitro RBE values are not always predictive of in vivo RBE. We assume that this discrepancy stems from the fact that in vitro clonogenicity serves only as a proxy to the complex biological dynamics of tissue and tumor dose response. These differences in dose response and RBE most likely originate from

two sources: Firstly, environmental differences (lack of tissue context, presence of artificial structures, altered nutrient availability, relatively low cell density) alter the biological response. Secondly, method-related biases caused by experimental design decisions such as time of readout and viability size thresholds might influence the results differently depending on radiation modality. While the environmental differences remain, the presented method could help to match in vitro RBE results to in vivo RBE results by reducing the method-related biases. To which extend this is possible is a question for future research projects. Despite the large variability in threshold-based quantification of clonogenic survival and the systematic biases observed here, the IVCA is still a valid method for survival quantification. Experienced experimentalists using well-characterized cell lines can achieve quantitative results with considerably lower variability than seen in our data. However, the potential influence of systematic misclassification and bias cannot be ruled out by the standard method alone. Using the trIVCA analysis, such experiments can be examined in detail and tested for potential misclassification and bias.

As we only analyzed three cell lines, we do not claim generalizability of the observed trends. Assumptions about slow-growing clonogenic colonies and late abortive events might not be justified for other cell lines. However, to test these assumptions for other cell lines and conditions, we need to inspect colony growth behavior in a time-resolved manner as we do in the trIVCA analysis.

While the initial setup for experiment and analysis exceeds the effort for a standard IVCA, the framework is now established and can be applied in further studies. If an automated image acquisition system is available, the efforts to perform a trIVCA analysis are not substantially higher than for a classical IVCA but return considerably more information.

The classification of growth behavior and thus clonogenicity is less straightforward compared to the IVCA. Just as in the IVCA, it relies on the experimenter's assessment of classification. However, in contrast to manual count-based classification, the classifier model and its results are stored digitally and can be examined, retrained, and tested reproducibly.

A current limitation of the trIVCA method is the lack of precisely counted cell numbers. As the light contrast microscopy image data does not allow robust single-cell counting, we approximate the number of cells from a colony's area. This is a valid choice if cell sizes are consistent and colonies grow relatively flat, as for the cell lines in this work. If cell sizes are highly irregular, alternative imaging variants, potentially including fluorescence markers would be necessary to adapt the method.

Conclusion

We introduced the time-resolved in vitro clonogenic assay, yielding a growth behavior-based definition of clonogenicity which includes more, relevant information compared to the standard in vitro clonogenic assay. As this definition does not depend on the standard readout choices, it avoids potential bias and produces more accurate results.

Declaration of Competing Interest

The authors declare that they have no known competing financial interests or personal relationships that could have appeared to influence the work reported in this paper.

Acknowledgements

This work was supported by the Alois Hirdt–Erben und Wieland–-Stiftung. We give thanks to the Light Microscopy Facility at the German Cancer Research Center (DKFZ) Heidelberg for technical support.

Appendix A. Supplementary data

Supplementary data to this article can be found online at https://doi.org/10.1016/j.ctro.2023.100662.

References

[1] Puck TT, Marcus PI. Action of X-rays on Mammalian Cells. J Exp Med May 1956; 103(5):653–66. https://doi.org/10.1084/jem.103.5.653.
[2] Paganetti H. Relative biological effectiveness (RBE) values for proton beam therapy. Variations as a function of biological endpoint, dose, and linear energy transfer. Phys Med Biol Nov. 2014;59(22):R419–72. https://doi.org/10.1088/0031-9155/59/22/R419.
[3] Matsui T, Nuryadi E, Komatsu S, Hirota Y, Shibata A, Oike T, et al. Robustness of Clonogenic Assays as a Biomarker for Cancer Cell Radiosensitivity. Int J Mol Sci Aug. 2019;20(17):4148.
[4] Lumley MA, Burgess R, Billingham LJ, McDonald DF, Milligan DW. Colony counting is a Major Source of Variation in CFU-GM Results Between Centres. Br J Haematol May 1997;97(2):481–4. https://doi.org/10.1046/j.1365-2141.1997.492695.x.
[5] Biston M-C, Corde S, Camus E, Marti-Battle R, Estève F, Balosso J. An Objective Method to Measure Cell Survival by Computer-Assisted Image Processing of Numeric Images of Petri Dishes. Phys Med Biol Jun. 2003;48(11):1551–63. https://doi.org/10.1088/0031-9155/48/11/305.
[6] Brix N, Samaga D, Hennel R, Gehr K, Zitzelsberger H, Lauber K. The clonogenic assay: robustness of plating efficiency-based analysis is strongly compromised by cellular cooperation. Radiat Oncol Dec. 2020;15(1):248. https://doi.org/10.1186/s13014-020-01697-y.
[7] Jensen PB, Roed H, Vindelov L, Christensen IJ, Hansen HH. Reduced variation in the clonogenic assay obtained by standardization of the cell culture conditions prior to drug testing on human small cell lung cancer cell lines. Invest New Drugs Nov. 1989;7:307–15. https://doi.org/10.1007/BF00173760.
[8] Nuryadi E, Mayang Permata TB, Komatsu S, Oike T, Nakano T. Inter-assay precision of clonogenic assays for radiosensitivity in cancer cell line A549. Oncotarget Mar. 2018;9(17):13706–12. https://doi.org/10.18632/oncotarget.24448.
[9] Koch RA, Harmel C, Alber M, Bahn E. A framework for automated time-resolved analysis of cell colony growth after irradiation. Phys Med Biol Feb. 2021;66(3):035017. https://doi.org/10.1088/1361-6560/abd00d.
[10] Franken NAP, Rodermond HM, Stap J, Haveman J, van Bree C. Clonogenic Assay of Cells in vitro. Nat Protoc Dec. 2006;1(5):2315–9. https://doi.org/10.1038/nprot.2006.339.
[11] Bronk L, Guan F, Patel D, Ma D, Kroger B, Wang X, et al. 'Mapping the Relative Biological Effectiveness of Proton, Helium and Carbon Ions with High-Throughput Techniques'. Cancers Dec. 2020;12(12):3658.
[12] Chalfoun J, Majurski M, Blattner T, Bhadriraju K, Keyrouz W, Bajcsy P, et al. MIST: Accurate and Scalable Microscopy Image Stitching Tool with Stage Modeling and Error Minimization. Sci Rep Dec. 2017;7(1). https://doi.org/10.1038/s41598-017-04567-y.
[13] Marstal K, Berendsen F, Staring M, Klein S. SimpleElastix: A User-Friendly, Multilingual Library for Medical Image Registration. In: *2016 IEEE Conference on Computer Vision and Pattern Recognition Workshops (CVPRW)*, Las Vegas. NV, USA: IEEE; Jun. 2016. p. 574–82. https://doi.org/10.1109/CVPRW.2016.78.
[14] Klein S, Staring M, Murphy K, Viergever MA, Pluim J. elastix: A Toolbox for Intensity-Based Medical Image Registration. IEEE Trans Med Imaging Jan. 2010;29(1):196–205. https://doi.org/10.1109/TMI.2009.2035616.
[15] Isensee F, Jaeger PF, Kohl SAA, Petersen J, Maier-Hein KH. nnU-Net: a self-configuring method for deep learning-based biomedical image segmentation. Nat Methods Feb. 2021;18(2):203–11. https://doi.org/10.1038/s41592-020-01008-z.
[16] napari contributors, 'napari: a multi-dimensional image viewer for python', *https://napari.org/stable/*, 2019, doi: 10.5281/zenodo.3555620.
[17] Hall EJ, Giaccia AJ. Radiobiology for the radiologist. 7th ed. Philadelphia: Wolters Kluwer Health/Lippincott Williams & Wilkins; 2012.
[18] Sinclair WK. X-Ray-Induced Heritable Damage (Small-Colony Formation) in Cultured Mammalian Cells. Radiat Res Apr. 1964;21(4):584–611. https://doi.org/10.2307/3571653.
[19] Joshi GP, Nelson WJ, Revell SH, Shaw CA. Discrimination of Slow Growth from Non-survival Among Small Colonies of Diploid Syrian Hamster Cells After Chromosome Damage Induced by a Range of X-ray Doses. Int J Radiat Biol Relat Stud Phys Chem Med Jan. 1982;42(3):283–96. https://doi.org/10.1080/09553008214551201.
[20] Nias AHW, Gilbert CW, Lajtha LG, Lange CS. Clone-size Analysis in the Study of Cell Growth Following Single or During Continuous Irradiation. Int J Radiat Biol Relat Stud Phys Chem Med Jan. 1965;9(3):275–90. https://doi.org/10.1080/09553006514550331.
[21] G. W. Barendsen, 'Responses Of Cultured Cells, Tumours, And Normal Tissues To Radiations Of Different Linear Energy Transfer.', *Pp 293-356 Curr. Top. Radiat. Res. Vol IV Ebert Michael Howard Alma Eds N. Y. John Wiley Sons Inc 1968*, Oct. 1968, Accessed: Jun. 05, 2023. [Online]. Available: https://www.osti.gov/biblio/4500126.